Original paper

Gamma-ray sources imaging and test-beam results with MACACO III Compton camera

L. Barrientos [a],[*], M. Borja-Lloret [a], J.V. Casaña [a], P. Dendooven [b], J. García López [c],[d], F. Hueso-González [a], M.C. Jiménez-Ramos [c],[e], J. Pérez-Curbelo [a], A. Ros [a], J. Roser [a], C. Senra [a], R. Viegas [a], G. Llosá [a]

[a] Instituto de Física Corpuscular (IFIC), CSIC-UV, Valencia, Spain
[b] Particle Therapy Research Center (PARTREC), Department of Radiation Oncology, University Medical Center Groningen, Groningen, The Netherlands
[c] Centro Nacional de Aceleradores (Universidad de Sevilla, CSIC and Junta de Andalucía), E-41092 Sevilla, Spain
[d] Departamento de Física Atómica, Molecular y Nuclear, Universidad de Sevilla, Sevilla, Spain
[e] Departamento de Física Aplicada II, Universidad de Sevilla, 41012 Sevilla, Spain

A B S T R A C T

Hadron therapy is a radiotherapy modality which offers a precise energy deposition to the tumors and a dose reduction to healthy tissue as compared to conventional methods. However, methods for real-time monitoring are required to ensure that the radiation dose is deposited on the target. The IRIS group of IFIC-Valencia developed a Compton camera prototype for this purpose, intending to image the Prompt Gammas emitted by the tissue during irradiation. The system detectors are composed of Lanthanum (III) bromide scintillator crystals coupled to silicon photomultipliers. After an initial characterization in the laboratory, in order to assess the system capabilities for future experiments in proton therapy centers, different tests were carried out in two facilities: PARTREC (Groningen, The Netherlands) and the CNA cyclotron (Sevilla, Spain). Characterization studies performed at PARTREC indicated that the detectors linearity was improved with respect to the previous version and an energy resolution of 5.2 % FWHM at 511 keV was achieved. Moreover, the imaging capabilities of the system were evaluated with a line source of ^{68}Ge and a point-like source of ^{241}Am-^{9}Be. Images at 4.439 MeV were obtained from irradiation of a graphite target with an 18 MeV proton beam at CNA, to perform a study of the system potential to detect shifts at different intensities. In this sense, the system was able to distinguish 1 mm variations in the target position at different beam current intensities for measurement times of 1800 and 600 s.

1. Introduction

Hadron therapy (HT) is a cancer treatment technique consisting of the irradiation of tumors with protons or other light ions. These particles, unlike the conventionally used photons, deposit most of their energy in a precise region known as Bragg peak which is dependent on the beam energy [1]. Nowadays, HT use has increased due to its advantage of maximizing the dose deposited on a tumor while reducing the toxicity of the treatment as compared to conventional radiotherapy. However, the physical characteristics of particles used in HT increase the complexity in terms of imaging accuracy and image-based dose calculation [2]. Therefore, the current practice is carried out by using safety margins [3] to consider the possible sources of uncertainty associated to the treatment [4]. Verification techniques of treatment delivery are required to fully exploit the advantages of

this type of therapy in the clinical setting [5]. In this sense, Compton cameras (CCs) have emerged as possible candidates for monitoring HT [6]. CCs are gamma-ray imaging systems currently considered as an option for different approaches in medical imaging [7–10]. In these areas, Compton imaging technology is still in the development phase, thus it is not used in clinical practice [11]. Nevertheless, the ongoing development and the wide variety of materials used as detectors in CCs allow further improvement of their performance. Thus, a variety of CCs for HT treatment monitoring have been developed by several research groups with different materials [12–14], and geometries [15,16]. In this line, the IRIS group of IFIC-Valencia has developed a third version of a Compton camera prototype (MACACO: Medical Applications CompAct COmpton camera). Experimental tests with the system in the laboratory [17] evidenced an improved performance over the previous

versions of the prototype [18,19]. After the system characterization at low photon energies with point-like sources, experimental tests with high energy photons have been carried out in two different facilities: The Particle Therapy Research Center (PARTREC, formerly KVI-CART), University of Groningen, The Netherlands and the Centro Nacional de Aceleradores (CNA), Sevilla, Spain. This work presents results from these two measurement campaigns: In first place, the system response was evaluated at PARTREC with sources of different energies and geometries. Tests in the proton beam at CNA using different current intensities were performed, where analysis was limited to prompt gamma ray (PG) with an energy of 4.439 MeV. Tests performed in the first facility involved calibration of the detectors, as well as assessment of the system response and imaging capabilities with ^{68}Ge and ^{241}Am-^{9}Be sources, including measurements with 4.4 MeV photons, which represents a relevant energy in PG production. MACACO III has also been tested at CNA with a proton beam of 18 MeV impinging on a graphite target to produce photons of 4.439 MeV. Data have been taken displacing the prompt gamma source to quantify the CC ability to distinguish range shifts in the proton beam. Moreover, the measurements were acquired at different beam intensities in an attempt to approach clinical intensities and establish a comparison with the previous version of the system [20]. The results presented in this work are aimed at testing the system at high photon energies (above 1 MeV), which are relevant for hadron therapy treatment monitoring, but can also be of use in other gamma-ray imaging applications such as medical imaging [21–23] or identification of radioactive isotopes [24].

2. Materials and methods

2.1. Prototype description

The CC prototype comprises three detector layers made of Lanthanum (III) bromide (LaBr$_3$) scintillator crystals and silicon photomultipliers (SiPMs). The system can be operated with two or three detectors, without requiring absorption, which favors its use in applications with high-energy photons. Each detector plane is composed of a monolithic LaBr$_3$ crystal from Saint Gobain with dimensions of $25.8 \times 25.8 \times 5$ mm^3 coupled to a SiPM array S13360-3025CS from Hamamatsu Photonics. Both elements are plugged into a printed circuit board (PCB) that contains the VATA64HDR16 ASIC from Ideas [25]. This readout chip is responsible for reading and processing the signal collected by each of the 64 SiPM elements. The features and capabilities of the selected ASIC are described in [26], where a thorough characterization study has been performed. The PCBs of the prototype are designed to provide mechanical support to each of the detectors as well as the SiPMs bias voltage. In this case, The PCBs are connected to a programmable power supply specifically made for powering all the system detectors [27]. The AliVATA board equipped with a Spartan 6 Field Programmable Gate Arrays described in [17] operates the system detectors. The AliVATA acquisition process is controlled by a dedicated software known as Vdaq, that allows to set different detector parameters before or during measurement runs. This in-house developed software features a graphical user interface based on the VMEDAQ framework [28], which permits data acquisition in singles or time coincidence mode. To operate the detectors in time coincidence, the prototype uses a dedicated board that allows simultaneous measurement of two and three coincidence events [29]. The evaluation board is a Virtex 5 FPGA programmed with the OR logic, i.e., an output signal is generated when two or more detector trigger signals overlap. In addition to the described CC prototype, a reference detector was also used for the acquisition of the energy spectra from gamma-ray sources used in this work. This detector comprises a LaBr$_3$ crystal of $51.2 \times 51.2 \times 10$ mm^3 coupled to a photomultiplier tube (PMT) model R6237 from Hamamatsu photonics positioned always in the CC line of sight.

2.2. Measurements

The study of the detectors' response at different energies and the acquisition of in-beam data were carried out at two different facilities. In one case with radioactive sources whereas in another with a proton beam, as described below.

2.2.1. Tests with radioactive sources at PARTREC

The calibration, evaluation of detector response at high energies and imaging tests were addressed at PARTREC, Groningen. The radioactive sources employed were a 183 mm long ^{68}Ge line source and a ^{241}Am-^{9}Be point-like source with activities of 0.64 and 37 MBq, respectively. The ^{68}Ge source allows evaluating the system response with extensive sources at 511 and 1077 keV while the ^{241}Am-^{9}Be source allows to focus the study on 4.4 MeV photons. Such photons are produced as a consequence of the interaction between an α particle with the beryllium through the reaction ^{9}Be(α, n) ^{12}C, also generating a neutron in the process [5]. Fig. 1(a) shows a picture of the Compton camera experimental setup with the line source of ^{68}Ge and the PMT detector placed below the CC detectors. The measurements were taken with the sources placed at 70 mm from the first detector of the CC and an inter-plane distance (center to center) of 50 mm [17]. Fig. 1(b) shows a block diagram of the system geometrical configuration with the two sources employed in the experiment. The singles measurements were used for detector calibration, as well as to determine the energy resolution and evaluate the linearity of the detectors. In this sense, the energy resolution was determined by performing a Gaussian fit of the photopeaks, while the linearity was studied by plotting the photopeak positions versus the photon energy. Considering the different features of the sources used in terms of dimensions and emission energies, coincidences data were used to reconstruct the source distribution in different circumstances. The ^{68}Ge reconstruction was carried out using the most energetic photons (1077 keV) as a performance indicator of the accuracy in the CC position reconstruction. In the case of the ^{241}Am-^{9}Be source, the reconstruction was performed to evaluate the imaging capability of the system at 4.4 MeV, which corresponds to a relevant energy for PG detection.

2.2.2. In-beam measurements at CNA

Measurements with the Compton camera in a proton beam have been carried out at CNA, Sevilla. The employed cyclotron is a Cyclone 18/9 from IBA [30] which allows accelerating protons and deuterons up to 18 and 9 MeV, respectively [31]. Tests with MACACO III were carried out in the same way as with the previous version of the system [20] and with another CC prototype developed by the group (MACACOp) [30]. All these experiments were performed with an 18 MeV proton beam impinging on a graphite target to produce 4.439 MeV gamma-rays, arising from the inelastic ^{12}C(p,p')^{12}C* reaction. In this case, the target consists of a plate with dimensions of 80×400 mm^2 and 3.6 mm thickness located at 110 mm from the proton beam exit. Fig. 2(a) shows a picture of the experimental setup with the graphite target placed in the beam direction (*x*-axis). The Compton camera and the PMT reference detector were located perpendicularly to the beam line. Fig. 2(b) shows a block diagram of the geometrical arrangement of the experiment performed at CNA. The distance from the graphite target to the Compton camera was 130 mm while the detectors planes were separated by an inter-plane distance of 50 mm. In this case, the choice of the source distance is related to avoid detectors' saturation and prevent direct protons from reaching them. The photon emission distribution resulting from the irradiation of the graphite target was obtained at three different beam current intensities: low intensity of 0.25 nA, medium intensity of 2.5 nA and high intensity of 3.9 nA. These quantities are equivalent to a total emission rate of 1.6, 15.6 and 24.4×10^9 protons per second. For the measurements, the graphite target was placed at different positions (on *x*-axis) separated at 1 mm by means of a motorized linear stage with a micrometric precision of
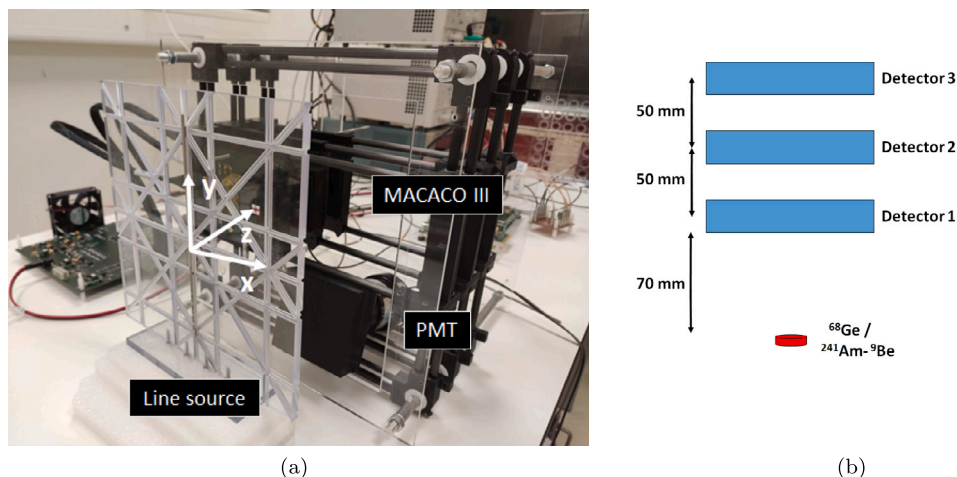
Fig. 1. Images of the experimental setup of MACACO III Compton camera at PARTREC. (a) Picture of the MACACO III system with the PMT placed in the same direction as the CC detectors, where the line source of ^{68}Ge can be seen in vertical position. (b) Block diagram of the measurements setup with the radioactive sources.
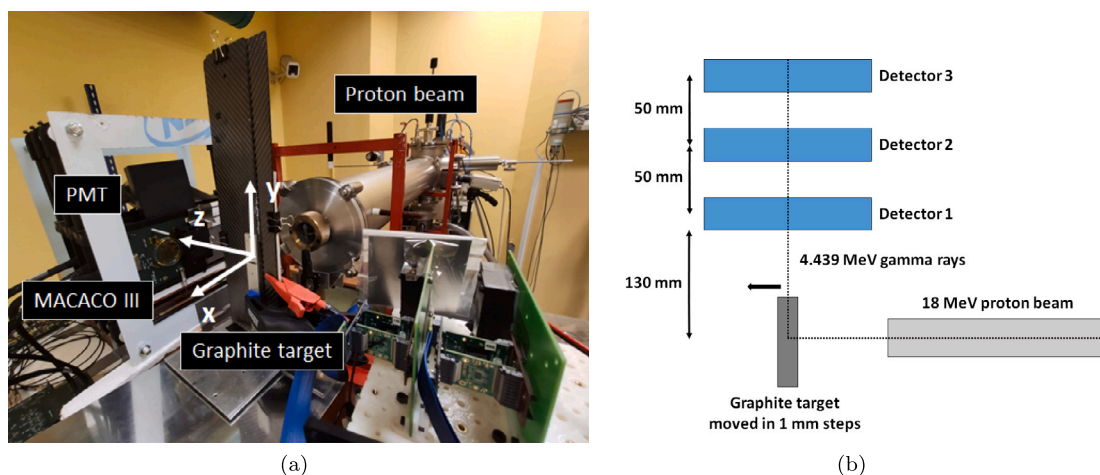

Fig. 2. Images of the test-beam performed with the CC prototype. (a) Experimental setup: proton beam, graphite target, Compton camera (left side of the image) and PMT (placed over the CC detectors) can be seen. (b) Schematic drawing of the in-beam measurements carried out at CNA.

± 80 µm. As described in Section 2.2.1, singles and coincidences data were taken for different purposes. In the case of singles measurements, these were used for data calibration and to perform a comparison with the spectrum measured by the PMT, while coincidences data were also employed for data calibration and image reconstruction. In this sense and to have sufficient events, the acquisition time of the measurements in singles mode was 120 s. For coincidences mode and considering the increase in the beam intensity, the measurement times were 1800, 600 and 300 s for the three cases. The distances between the reconstructed photon emission distributions were calculated using R80 and R50, which corresponds to the 80 % and 50 % of intensity after the maximum of the distribution [32].

2.3. Image reconstruction

Coincidences data of the different sources (^{68}Ge and ^{241}Am-^{9}Be) and the in-beam data presented in this work were acquired with the three detectors of the Compton camera. All images were reconstructed using the List Mode Maximum Likelihood Expectation Maximization (LM-MLEM) algorithm [33]. In the case of the ^{68}Ge images at 1077 keV (Section 2.2.1), the LM-MLEM was used in conjunction with the model based on analytical expressions of the sensitivity and system matrices described in [34]. For the image reconstruction of the ^{241}Am-^{9}Be source and in-beam data, the sensitivity and system matrices were

determined by means of a spectral analytical model detailed in [35]. In this work, the latter code yields four-dimensional (energy and position) images by using two- [35] and three-interaction events [36]. Such spectral reconstruction algorithm is better suited for PG imaging, as the incoming gamma-ray energy is not known beforehand. In all cases, images were obtained combining the events measured from the four channels of information of MACACO III, using the joint image reconstruction algorithm described in [37]. Energy windows have been introduced to eliminate contamination from the photons not required for the reconstruction process. Thus, in the ^{68}Ge case, the energy cut was introduced below 0.7 MeV whereas for the ^{241}Am-^{9}Be and the in-beam data these were applied below 1.6 and 0.8 MeV, respectively. In order to correctly visualize each of the reconstructed gamma sources, a maximum number of 50 iterations and different field-of-view (FOV) and voxel sizes were selected. Considering the different geometry of the sources presented in this work and defining a FOV large enough to contain them, a FOV of 81 × 201 × 33 with a voxel size of 3 × 1 × 3 mm^3 was employed for the ^{68}Ge. In the case of the ^{241}Am-^{9}Be source, a FOV of 61 × 61 × 33 mm^3 with 1 × 1 × 3 mm^3 voxel size was selected. For the in-beam data, a FOV of 48 × 23 × 13 mm^3 with a voxel size of 0.5 × 1 × 3 mm^3 was established, to identify the graphite target displacements in the x direction and perform a comparison with the results obtained with MACACOp at the same energy [30]. The spectral part of the FOV for the images involving photons of 4.439 MeV
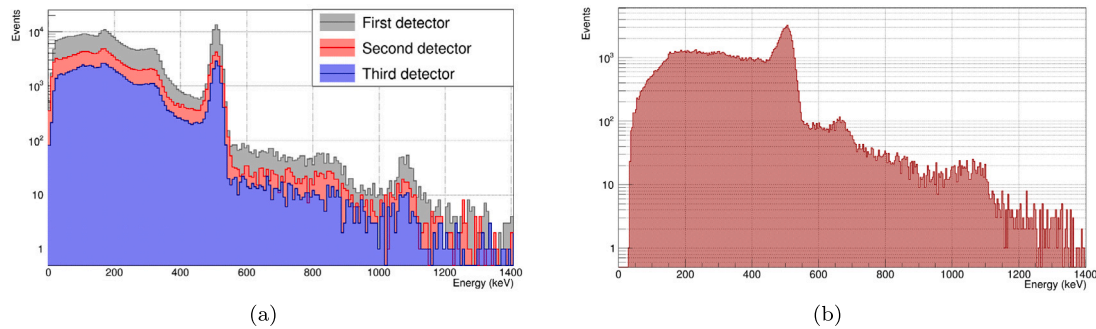
Fig. 3. Energy spectra of ^{68}Ge measured with MACACO III in (a) Singles. (b) Coincidences mode (sum spectrum).

corresponds to 10 bins covering an energy range from 0.2 to 8.0 MeV. In order to suppress noise as well as improve the visualization of the images, a median filter was applied after the final iteration.

3. Results

3.1. Tests at PARTREC

3.1.1. Detector characterization

The following section shows spectra of different radioactive sources (Section 2.2.1) acquired with the CC to study its response at different energies.

Results with ^{68}Ge

First, the study of the system response and the calibration were performed at 511 and 1077 keV using the line source of ^{68}Ge described above. Fig. 3 shows the corresponding spectra in singles and coincidences mode measured by the system. Fig. 3(a) shows the ^{68}Ge singles spectra of the three CC detectors in the same plot. The energy resolution achieved applying a bias voltage of 55.4 V was 5.2%, 5.6% and 5.2% FWHM at 511 keV and 4.3%, 5.1% and 4.3% FWHM at 1077 keV for planes 1 to 3, respectively. Fig. 3(b) shows an energy spectrum of ^{68}Ge resulting from summing the energies deposited by the photons in the coincidences between the first and the second detector. The gamma emissions of 511 and 1077 keV can be clearly noted, as well as a photopeak located at 681 keV derived from the simultaneous absorption of photons with energies of 511 and 170 keV (backscatter events).

^{241}Am-^{9}Be

The calibration of the detectors with a point-like source of ^{241}Am-^{9}Be has also been carried out, to study the system response at 4.4 MeV for the subsequent in-beam measurements with PG of this energy. Fig. 4 shows the results obtained in singles and coincidences mode with the ^{241}Am-^{9}Be source (see Section 2.2.1). Fig. 4(a) shows different spectra of the point-like source in singles mode with the three detectors. The ASIC's limited dynamic range (-20 to 55 pC) affects the energy response of the system at 4.4 MeV producing detector saturation and resulting in degraded spectra, where only the 511 keV annihilation photopeak can be barely seen. As a consequence, it is not possible to distinguish the 4.4 MeV photopeak nor the single and double escape peaks located at $\approx$3.9 and 3.4 MeV, respectively. These two lower energy photopeaks are a consequence of a pair production process, in which one or two 511 keV photons have escaped from the detector. However, from 3 MeV onward, a region with a higher accumulation of events which corresponds to these three photopeaks can be seen in the spectra. In this study and for the energy calibrations with 4.4 MeV photons, the highest part of this region represents the 3.4 MeV photopeak, which is the most likely of the three ones. The photopeaks of the spectra measured by the second and third detector are widened with respect to the one measured in the first detector. This is mainly due to photons

scattering in the first or second detectors (or with passive material) before being absorbed in the second and third detectors. Fig. 4(b) shows a spectrum formed by the sum of the energies measured in the first and the second detector, the most relevant channel for the reconstruction process due to its higher statistics. The spectrum of ^{241}Am-^{9}Be exhibits the same trend as the ones shown in Fig. 4(a), which corresponds to a continuum of different energies. Fig. 4(c) shows the position in ADC units of the visible photopeaks of the ^{241}Am-^{9}Be source (511 and 3400 keV) combined with the ^{68}Ge ones (511 and 1077 keV) as a function of their respective energies, in which a linear fit was applied to the data.

3.1.2. Radioactive source imaging

The results of this section correspond to the imaging tests performed with the gamma-ray sources described in Section 3.1.1.

^{68}Ge

The ^{68}Ge line source was imaged with the CC geometrical configuration mentioned above. As explained in Section 2.3, image reconstruction was performed using the event combination from the different CC detector planes considering all double and triple coincidences. Fig. 5 shows the reconstructed image of the ^{68}Ge line source in vertical position with respect to the system detectors. The line source has been reconstructed introducing an energy cut for photon energies below 700 keV to select those photons with initial energy of 1077 keV. Fig. 5(a) shows an xy-slice of the ^{68}Ge source image reconstructed using photons of this energy. The orange square included in the plot represents the footprint of the detectors. Despite their limited size, the line source has been reconstructed to a large extent, although not fully recovering its length. This could be due to a low detection probability of photons emitted with high angles coming from the source edges given the small CC detectors size. Fig. 5(b) shows a plot of the recovered intensity as a function of the y-axis direction from image 5(a). It is possible to observe that $\approx$126 mm (marked within a blue square) out of a total active length of 183 mm has been successfully recovered. This quantity has been estimated from the recovered intensity values that exceed a threshold of 0.2 arbitrary units. The choice of the value is related to the fact that the background noise for the reconstructed image is around 0.15 (which can be appreciated for y-coordinates -90 to -100 mm).

^{241}Am-^{9}Be

To evaluate the system imaging capabilities at 4.4 MeV in view of the experiments performed with a proton beam (Section 2.2.2), the ^{241}Am-^{9}Be source was imaged using the spectral code mentioned above. Fig. 6 shows different slices of the 4D image reconstructed from the data combined from the acquisition with two and three detectors. Fig. 6(a) shows an xy-slice of the ^{241}Am-^{9}Be source at the spectral voxel containing 4.4 MeV after selecting those events with total energy deposition over 1.6 MeV. The point-like source has been correctly reconstructed without assuming previous knowledge of the initial energy of the emitted gamma-rays. Fig. 6(b) shows a 3D plot corresponding to an xE-slice from the 4D image of ^{241}Am-^{9}Be. A distribution centered at 4.4 MeV was obtained as a result of applying the spectral reconstruction code.

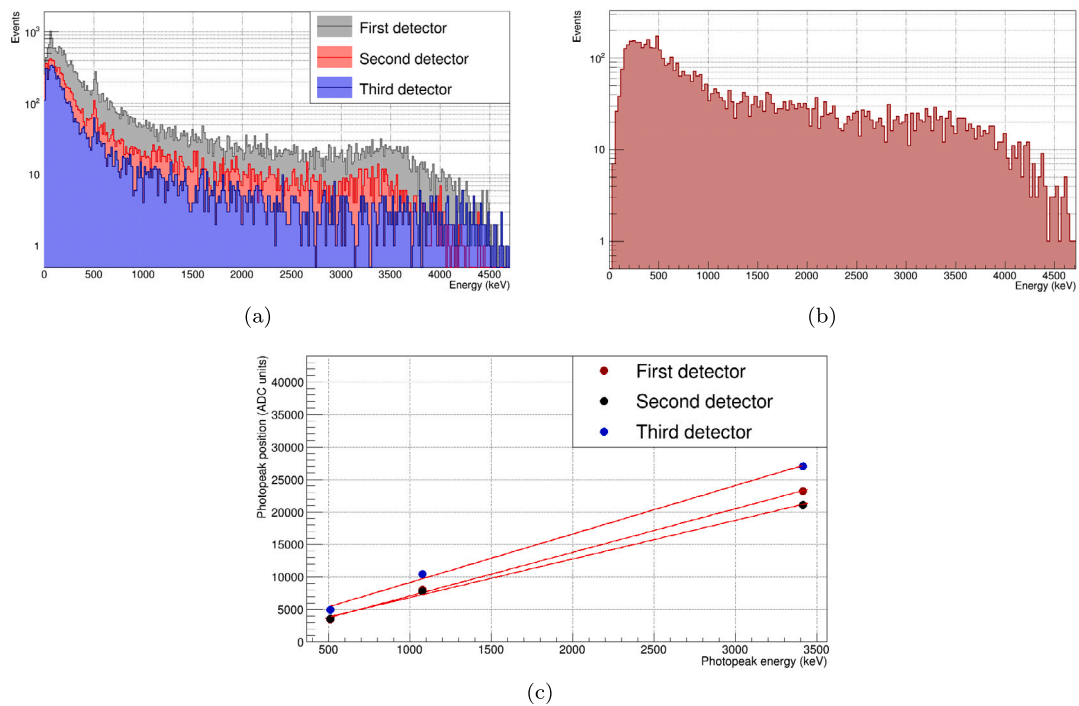**Fig. 4.** Detector characterization measurements, the ^{241}Am-^{9}Be data were calibrated using a linear fit for the photopeaks of 511 keV, 3.4 MeV and 1077 keV from the ^{68}Ge. (a) Calibrated ^{241}Am-^{9}Be spectra measured with the three system detectors in singles mode. (b) Coincidences (sum of energies measured in the first and the second detector). (c) Photopeaks position in ADC units versus photopeaks energy in keV for the data combined of ^{241}Am-^{9}Be and ^{68}Ge.
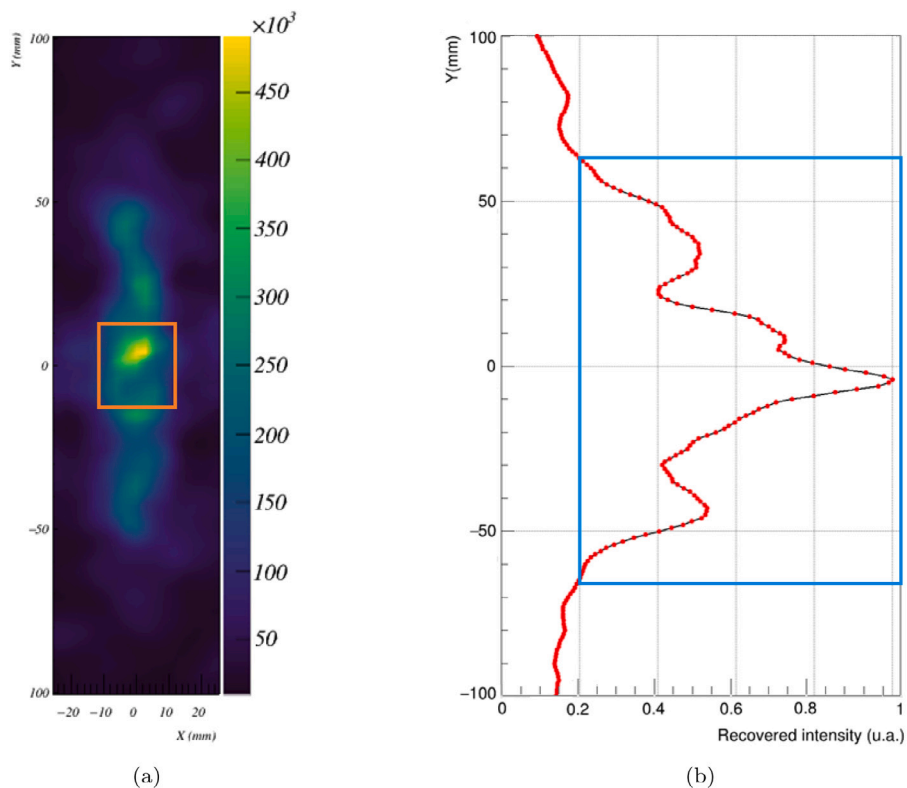

Fig. 5. ^{68}Ge source reconstructed images at 1077 keV using the combination of two and three interaction events. (a) *xy*-slice of the line source placed in vertical position. The lack of information relative to the recovered intensity could be a consequence of a low detection of events that are far away from the footprint of the detectors, shown by the orange square. (b) Plot of the *y*-projection of the image shown in (a) as a function of the intensity in arbitrary units. The blue square included in the plot represents the recovered length of the ^{68}Ge source.
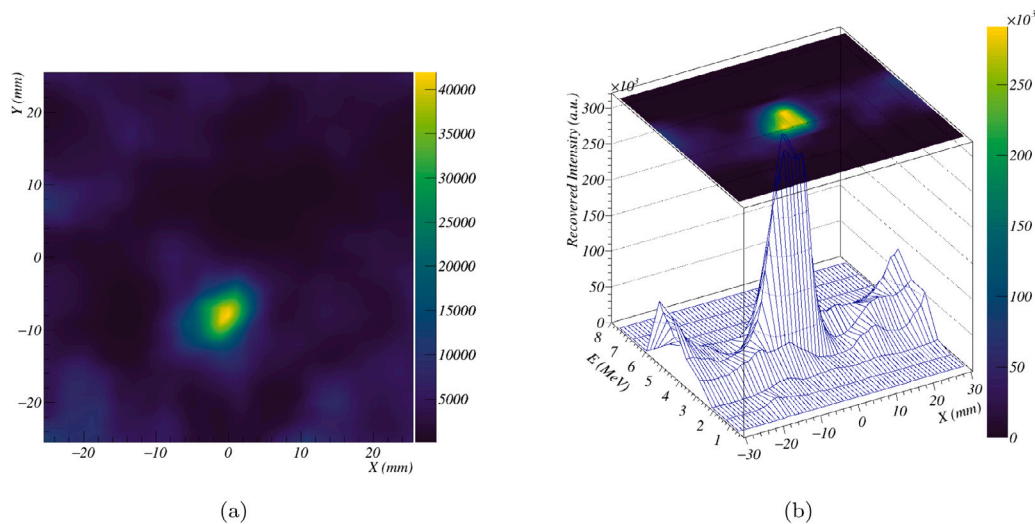
Fig. 6. ²⁴¹Am-⁹Be reconstructed 4D image at 4.4 MeV. (a) *xy*-slice of the reconstructed point-like source employing the coincidence events measured in two and three planes mode during 1200 seconds. (b) *xE*-slice as a function of the recovered intensity.

Table 1
Graphite target position, absolute positions and position difference of the R80 and the R50 of the reconstructed distributions with high-energy photons.

Beam current (nA)	Target position	Absolute position (± 0.25 mm)		Position difference (± 0.50 mm)	
		R50	R80	R50	R80
0.25	1	0.03	−1.04	–	–
	2	1.23	0.19	1.20	1.23
	3	2.47	1.12	1.24	0.93
2.5	1	−0.90	−2.78	–	–
	2	0.31	−1.59	1.21	1.19
	3	1.25	−0.58	0.94	1.01
3.9	1	3.12	2.02	–	–
	2	3.26	0.06	0.14	1.96

3.2. Tests at CNA

3.2.1. Detector characterization

This section shows energy spectra of the gamma rays induced by the proton beam acquired with the PMT reference detector and the CC.

Beam data

The system response at 4.439 MeV was also studied using the data taken from the beam described in Section 2.2.2. Fig. 7 shows the singles spectra produced after irradiation of a graphite target with the 18 MeV proton beam. Fig. 7(a) shows a beam spectrum at low current intensity (0.25 nA) acquired with the PMT reference detector placed within line of sight of the CC detectors. Different energy contributions can be distinguished as a result of the 4.439 MeV photons' interaction with the detector, such as the single and the double escape peak located at 3.928 and 3.417 MeV, respectively. In addition, a photopeak of 718 keV corresponding to PG of ^{12}C induced by reactions of protons on the graphite target can be clearly observed. Fig. 7(b) shows the beam spectrum at low intensity from image 7(a) but measured with the detectors of the CC. With the CC detectors, the measured spectra are degraded due to the limited dynamic range of the ASIC. Only three energy contributions are visible corresponding to 511 keV, 718 keV and a region that contains the three photopeaks associated to 4.439 MeV photons. Based on the measurements with PMT from Fig. 7(a) and as mentioned in Section 3.1.1, the point with the highest accumulation of events represents the single escape peak (3.417 MeV). In this case, and also considering the limited size of the detectors, the other two peaks (3.928 and 4.439 MeV) are not noticeable since the photon escape probability is higher as the incident energy increases. Fig. 7(c) shows the beam spectrum at high current intensity (3.9 nA) measured with the

PMT detector. As a result of the increase in the beam current intensity and contrast to the low intensity case, only three different contributions (511, 718 and 3417 keV) are visible from the spectrum. The loss of the remaining photopeaks is produced by the saturation of the PMT detector induced by pile-up effect, which produces spectrum degradation. Fig. 7(d) shows the spectra measured by the three system detectors with a nominal beam intensity of 3.9 nA. The spectra exhibit the same trend as the low intensity case, although the 511 keV photopeak widening is observed, essentially produced by pile-up, that affects the energy of the measured event.

3.2.2. Test-beam imaging

The results shown in the following section include the images reconstructed with beam data at different current intensities (0.25, 2.5 and 3.9 nA).

Low intensity

Fig. 8 shows the test-beam results obtained with MACACO III in coincidences mode at 4.439 MeV with an average beam current of 0.25 nA and an acquisition time of 1800 s. Figs. 8(a), 8(b) and 8(c) show reconstructed images from the photon emission distribution during proton irradiation of the graphite target at three different positions 1 mm apart. Image reconstruction was performed by selecting 30,000 events and using the combination of these from the different CC detector planes considering all the double and triple coincidences, as explained in Section 2.3. Fig. 8(d) shows line profiles along the *x*-axis from reconstructed images for the different graphite positions. The average separation distance between the three recovered spots using the R50 and R80 criteria was 1.1 ± 0.5 mm and 1.2 ± 0.5 mm, respectively (see Table 1).
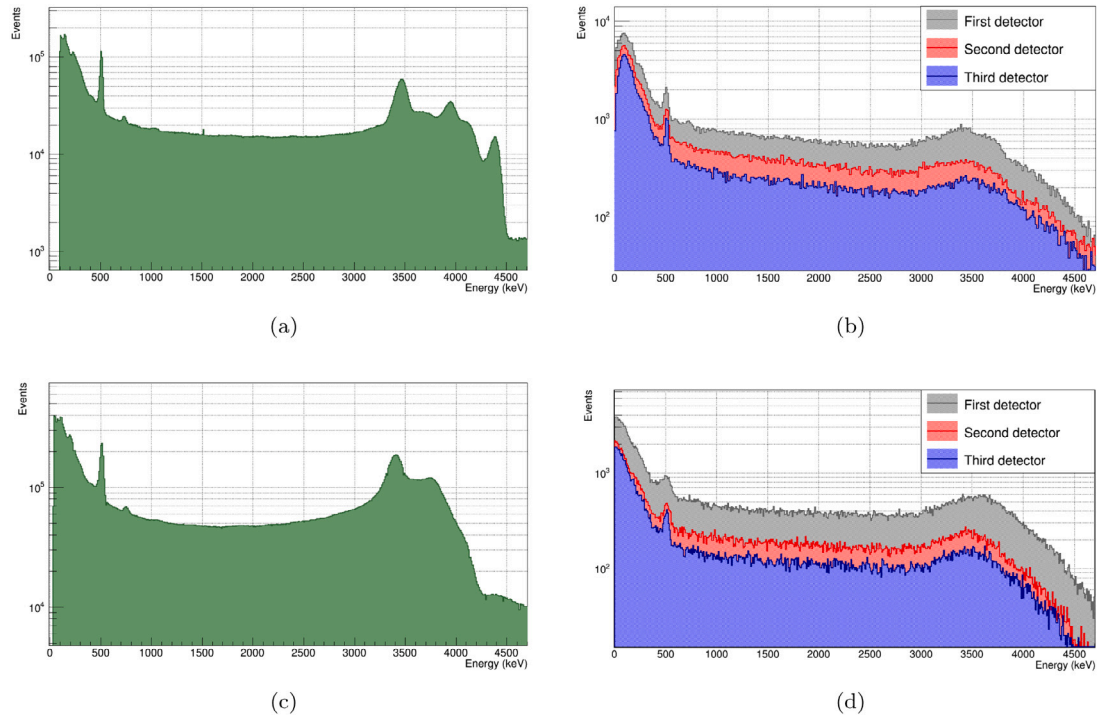
Fig. 7. Proton beam singles spectra measured with the (a) PMT detector at low intensity (0.25 nA). (b) Three detectors of MACACO III at low intensity. (c) PMT at high intensity (3.9 nA). (d) MACACO III detectors at high intensity.
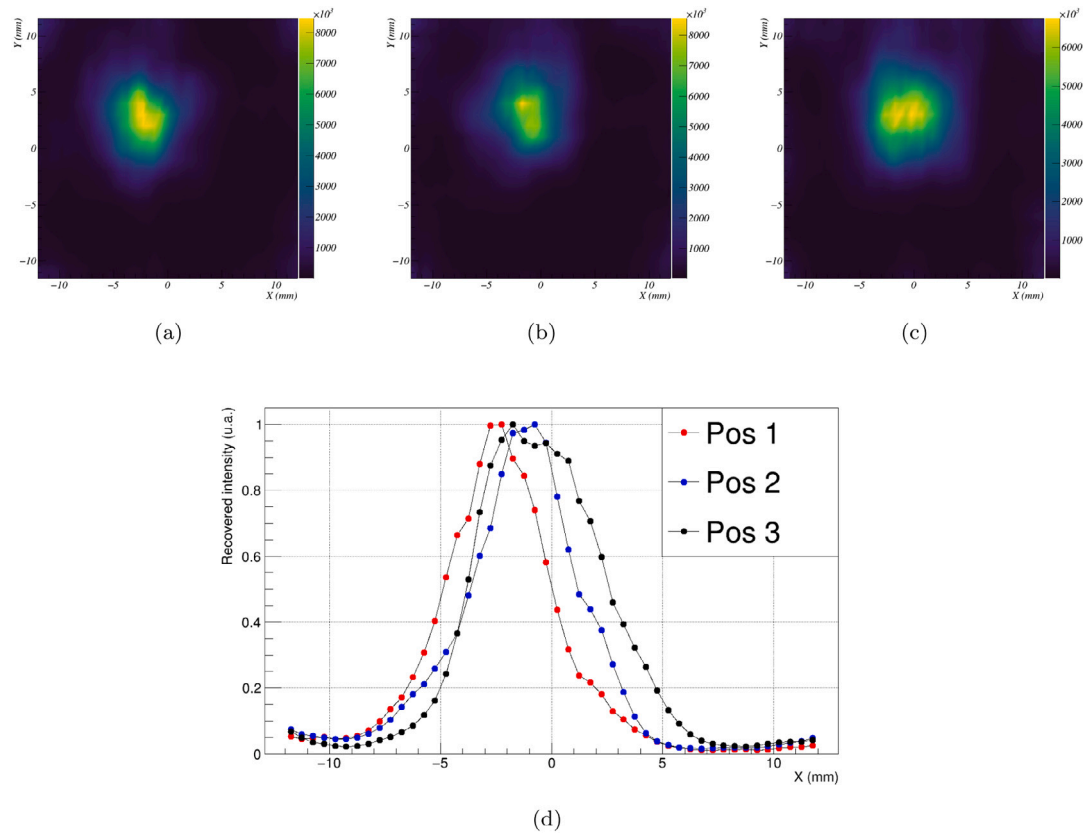

Fig. 8. Reconstructed images at 4.439 MeV measured with a nominal beam current intensity of 0.25 nA during 1800 s for three different graphite positions. (a) *xy*-slices of the photon emission distribution in Position 1. (b) Position 2. (c) Position 3. (d) Horizontal line profile through the maximum intensity point of the reconstructed images.
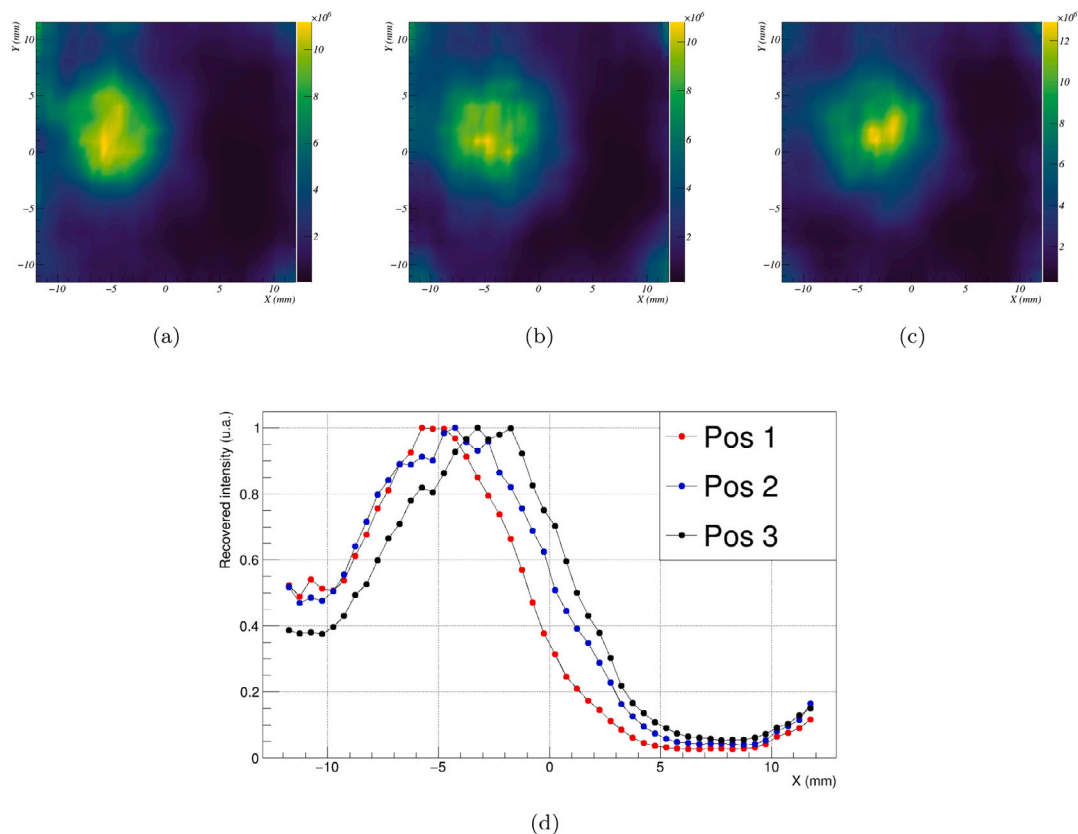
(a)   (b)   (c)

(d)

Fig. 9. Reconstructed images at 4.439 MeV acquired with a beam current intensity of 2.5 nA during 600 s for three different target positions. In this case, the total number of events considered in the image reconstruction was 1,000,000. (a) *xy*-slices of the PG emission distribution in Position 1. (b) Position 2. (c) Position 3. (d) Line profiles over the peak of the plot of the different target positions measured.

Medium intensity

Fig. 9 shows the reconstructed images at 4.439 MeV with a nominal beam intensity of 2.5 nA and a measurement time of 600 s. As in the previous case, Figs. 9(a), 9(b) and 9(c) show the photon emission distributions corresponding to the measured positions of the graphite target (Section 2.2.2). As a result of the higher beam intensity compared to Fig. 8, the FWHM of the reconstructed spots increases probably as a consequence of pile-up effect, that produces an energy overestimation of the measured events thus affecting image quality. Fig. 9(d) shows horizontal line profiles of the reconstructed images for the three different graphite positions. Still, as the low intensity case, it is also possible to distinguish target displacements of ≈1 mm using the criteria of the R50 and the R80. In this case, the average separation distance of the three spots using both criteria was of 1.1 ± 0.5 mm.

High intensity

The distributions of 4.439 MeV gamma rays generated by the graphite target at two positions 2 mm apart with a nominal intensity of 3.9 nA and a measurement time of 300 s were also reconstructed. However, unlike the previous cases and given by the system proximity to the target, the reconstructed beam spot is completely degraded and some artifacts are evidenced. The R80 and R50 of the two distributions have not shown reasonable changes in accordance with the target shift due to the saturation of the detectors and subsequent reconstructed spot degradation. The target position as well as the R80 and the R50 of the reconstructed images at low (Section 3.2.2), medium (Section 3.2.2) and high intensities are shown in Table 1.

4. Discussion

The CC prototype has been able to correctly generate images from high energy radioactive sources with different geometrical features.

This comprises line and point-like sources, as well as from the irradiation of a graphite target with a proton beam. Characterization studies at PARTREC with ^{68}Ge and ^{241}Am-^{9}Be sources indicate that the linearity of the detectors has improved with respect to previous versions of the system. In terms of energy resolution, we have achieved values of 5.2, 5.6 and 5.2% FWHM at 511 keV for the three detectors respectively, thus validating the results obtained previously [17].

Imaging tests with the line source of ^{68}Ge confirm the system potential to reconstruct sources significantly longer than the footprint of the detectors. In this sense, the line source of 183 mm has been imaged, fully recovering ≈68% of its active length in the process. The loss of the remaining 57 mm could be associated to a low detection of events with high angles emitted far away from the footprint of the detectors, from the source edges. Under the current prototype conditions, this would set the experimental limit of the CC MACACO III for the used geometrical configuration. In order to overcome this disadvantage, increasing the area of the detectors can be an option to solve the problem. In this context, the group is already working on an enhancement of the detector size that will allow us to have four times the size of the current ones.

Saturation of the detectors caused by the limited ASIC dynamic range [38] has been observed when measuring with the ^{241}Am-^{9}Be point-like source, where only a continuum of energies has been distinguished. In spite of the above, we have been able to successfully reconstruct the images using the spectral code described in [35], obtaining a spot located at 4.4 MeV.

From the in-beam data taken at CNA, spots of 4.439 MeV corresponding to the PG emission distribution have been successfully obtained at different beam current intensities. The measured spectra with the system as a result of the graphite target irradiation are quite different to the ones measured with the PMT detector. This could be

related to the dynamic range of the ASIC. An alternative to solve this problem could be the incorporation on the system of an ASIC with larger dynamic ranges features [30]. Also from the proton beam data, the system is able to discern one millimeter variations in the target positions for beam current intensities of 0.25 and 2.5 nA (using the R80 and the R50 criteria). The latter represents an improvement with respect to other published works with the Compton cameras MACACOp [30] and MACACO II [20]. However, for 3.9 nA of beam intensity and for a distance of 130 mm from the graphite target, the CC detectors exhibit saturation, which results in degraded spots ().

The joint reconstruction algorithm [37] has proven to be an enhanced complement relative to the methods employed in previous works [19,39]. The system has exhibited a substantial improvement in terms of imaging capability with different gamma-ray sources relative to previously obtained with its predecessors. The results presented in this article also open up the possibility to explore the system performance in other applications related to the medical imaging field. Thus, further work will include more measurement campaigns with proton beams for clinical use in HT facilities as well as tests with radiopharmaceuticals for nuclear medicine.

5. Conclusion and future work

The prototype shows a great versatility of application, since it is able to produce images from different low and high-energy sources (line, point-like and PG). In addition, MACACO III successfully generates in-beam images using all its detection channels jointly and differentiates 1 mm variations in the target position at relevant beam intensities, but low proton beam energies. However, the readout electronics employed has limitations to reach the required performance for the application in HT treatment monitoring. An alternative CC prototype known as MACACOp based on the TOFPET2 ASIC has been developed to improve the timing capabilities of the system, as well as the dynamic range and readout speed. Further work includes the development of larger detectors to increase the system efficiency and measurement campaigns in proton therapy centers.

Declaration of competing interest

The authors declare that they have no known competing financial interests or personal relationships that could have appeared to influence the work reported in this paper.

Acknowledgments

References

[1] Wilson RR. Radiological use of fast protons. Radiology 1946;47:487–91. http://dx.doi.org/10.1148/47.5.487.

[2] Thariat J, et al. Imaging issues specific to hadrontherapy (proton, carbon, helium therapy and other charged particles) for radiotherapy planning, setup, dose monitoring and tissue response assessment. Cancer Radiothér 2020;24:429–36. http://dx.doi.org/10.1016/j.canrad.2020.01.010.

[3] Albertini F, et al. Is it necessary to plan with safety margins for actively scanned proton therapy? Phys Med Biol 2011;56:4399. http://dx.doi.org/10.1088/0031-9155/56/14/011.

[4] Paganetti H, et al. Range uncertainties in proton therapy and the role of Monte Carlo simulations. Phys Med Biol 2012;57:R99. http://dx.doi.org/10.1088/0031-9155/57/11/R99.

[5] Solevi P, et al. Performance of MACACO compton telescope for ion-beam therapy monitoring: first test with proton beams. Phys Med Biol 2016;61:5149. http://dx.doi.org/10.1088/0031-9155/61/14/5149.

[6] Krimmer J, et al. Prompt-gamma monitoring in hadrontherapy: A review. Nucl Instrum Methods Phys Res A 2018;878:58–73. http://dx.doi.org/10.1016/j.nima.2017.07.063.

[7] Fujieda K, et al. First demonstration of portable compton camera to visualize 223-Ra concentration for radionuclide therapy. Nucl Instrum Methods Phys Res A 2020;958:162802. http://dx.doi.org/10.1016/j.nima.2019.162802.

[8] Shimazoe K, et al. Development of simultaneous PET and compton imaging using GAGG-SiPM based pixel detectors. Nucl Instrum Methods Phys Res A 2020;954:161499. http://dx.doi.org/10.1016/j.nima.2018.10.177.

[9] Liprandi S, et al. Sub-3mm spatial resolution from a large monolithic LaBr3 (Ce) scintillator. Curr Dir Biomed Eng 2017;3:655–9. http://dx.doi.org/10.1515/cdbme-2017-0138.

[10] Fontana M, et al. Compton camera study for high efficiency SPECT and benchmark with Anger system. Phys Med Biol 2017;62:8794. http://dx.doi.org/10.1088/1361-6560/aa926a.

[11] Tashima H, et al. Compton imaging for medical applications. Radiol Phys Technol 2022;15:187–205. http://dx.doi.org/10.1007/s12194-022-00666-2.

[12] Shiba S, et al. Use of a Si/CdTe compton camera for in vivo real-time monitoring of annihilation gamma rays generated by carbon ion beam irradiation. Front Oncol 2020;10:635. http://dx.doi.org/10.3389/fonc.2020.00635.

[13] Draeger E, et al. 3D prompt gamma imaging for proton beam range verification. Phys Med Biol 2018;63:035019. http://dx.doi.org/10.1088/1361-6560/aaa203.

[14] Aldawood S, et al. Development of a Compton camera for prompt-gamma medical imaging. Radiat Phys Chem 2017;140:190–7. http://dx.doi.org/10.1016/j.radphyschem.2017.01.024.

[15] Llosá G, et al. First images of a three-layer compton telescope prototype for treatment monitoring in hadron therapy. Front Oncol 2016;6:14. http://dx.doi.org/10.3389/fonc.2016.00014.

[16] Mccleskey M, et al. Evaluation of a multistage CdZnTe compton camera for prompt γ imaging for proton therapy. Nucl Instrum Methods Phys Res A 2015;785:163–9. http://dx.doi.org/10.1016/j.nima.2015.02.030.

[17] Barrientos L, et al. System characterization and performance studies with MACACO III Compton camera. Radiat Phys Chem 2023;208:110922. http://dx.doi.org/10.1016/j.radphyschem.2023.110922.

[18] Muñoz E, et al. Performance evaluation of MACACO: a multilayer compton camera. Phys Med Biol 2017;62:7321. http://dx.doi.org/10.1088/1361-6560/aa8070.

[19] Barrio J, et al. Performance improvement tests of MACACO: a compton telescope based on continuous crystals and SiPMs. Nucl Instrum Methods Phys Res A 2018;912:48–52. http://dx.doi.org/10.1016/j.nima.2017.10.033.

[20] Ros A, et al. MACACO II test-beam with high energy photons. Phys Med Biol 2020;65:245027. http://dx.doi.org/10.1088/1361-6560/abc5cd.

[21] Conka Nurdan T, et al. Design criteria for a high energy compton camera and possible application to targeted cancer therapy. J Instrum 2015;10:C07018. http://dx.doi.org/10.1088/1748-0221/10/07/C07018.

[22] Seo Y. Quantitative imaging of alpha-emitting therapeutic radiopharmaceuticals. Nucl Med Mol Imaging 2019;53:182–8. http://dx.doi.org/10.1007/s13139-019-00589-8.

[23] Yoshida E, et al. Whole gamma imaging: a new concept of PET combined with Compton imaging. Phys Med Biol 2020;65:125013. http://dx.doi.org/10.1088/1361-6560/ab8e89.

[24] Sato Y. Identification of depth location of a radiation source by measurement from only one direction using a Compton camera. Appl Radiat Isot 2023;195:110739. http://dx.doi.org/10.1016/j.apradiso.2023.110739.

[25] Meier D, et al. An ASIC for SiPM/MPPC readout. In: IEEE nucl. sci. symp. med. imag. conf.. 2010, p. 1653–7. http://dx.doi.org/10.1109/NSSMIC.2010.5874056.

[26] Barrio J, et al. Performance of VATA64HDR16 ASIC for medical physics applications based on continuous crystals and SiPMs. J Instrum 2015;10:P12001. http://dx.doi.org/10.1088/1748-0221/10/12/P12001.

[27] Querol M, et al. A programmable, multichannel power supply for SIPMs with temperature compensation loop and Ethernet interface. J Instrum 2016;11:C12035. http://dx.doi.org/10.1088/1748-0221/11/12/C12035.

[28] Stankova V, et al. Data acquisition system for the readout of SiPM matrix with the VATA64HDR16 front-end ASIC. In: IEEE nucl. sci. symp. med. imag. conf.. 2011, p. 807–9. http://dx.doi.org/10.1109/NSSMIC.2011.6154543.

[29] Muñoz E, et al. Tests of MACACO compton telescope with 4.44 MeV gamma rays. J Instrum 2018;13:P05007. http://dx.doi.org/10.1088/1748-0221/13/05/P05007.

[30] Viegas R, et al. Characterization of a Compton camera based on the TOF-PET2 ASIC. Radiat Phys Chem 2022;202:110507. http://dx.doi.org/10.1016/j.radphyschem.2022.110507.

[31] Baratto-Roldán A, et al. Feasibility study of a proton irradiation facility for radiobiological measurements at an 18 MeV cyclotron. Instruments 2018;2:26. http://dx.doi.org/10.3390/instruments2040026.

[32] Muñoz E, et al. Proton range verification with MACACO II compton camera enhanced by a neural network for event selection. Sci Rep 2021;11:1–12. http://dx.doi.org/10.1038/s41598-021-88812-5.

[33] Wilderman SJ, et al. Improved modeling of system response in list mode EM reconstruction of compton scatter camera images. IEEE Trans Nucl Sci 2001;48:111–6. http://dx.doi.org/10.1109/23.910840.

[34] Muñoz E, et al. Study and comparison of different sensitivity models for a two-plane Compton camera. Phys Med Biol 2018;63:13504. http://dx.doi.org/10.1088/1361-6560/aac8cd.

[35] Muñoz E, et al. A spectral reconstruction algorithm for two-plane Compton cameras. Phys Med Biol 2020;65:025011. http://dx.doi.org/10.1088/1361-6560/ab58ad.

[36] Roser J, et al. Image reconstruction for a multi-layer Compton telescope: an analytical model for three interaction events. Phys Med Biol 2020;65:145005. http://dx.doi.org/10.1088/1361-6560/ab8cd4.

[37] Roser J, et al. Joint image reconstruction algorithm in Compton cameras. Phys Med Biol 2022;67:155009. http://dx.doi.org/10.1088/1361-6560/ac7b08.

[38] Sánchez D, et al. HRFlexToT: a high dynamic range ASIC for time-of-flight positron emission tomography. IEEE Trans Radiat Plasma Med Sci 2021;6:51–67. http://dx.doi.org/10.1109/TRPMS.2021.3066426.

[39] Barrientos L, et al. Performance evaluation of MACACO II Compton camera. Nucl Instrum Methods Phys Res A 2021;1014:165702. http://dx.doi.org/10.1016/j.nima.2021.165702.